27th International Conference on Electrical Machines
Funchal, Madeira, Portugal | September 6-9, 2026

Paper Number ICEM26-000237

Nonlinear current control for synchronous machines with LC filter

Pascal Seitter and Christoph M. Hackl

Munich University of Applied Sciences (HM), Munich, Germany | {pascal.seitter, christoph.hackl}@hm.edu

Abstract

This study presents a nonlinear current control strategy for synchronous machines (SMs) equipped with an inverter-side LC filter. While LC filters attenuate the voltage harmonics of the pulse-width modulated inverter, they introduce additional dynamics and resonances into the drive system. The proposed approach employs input/output (I/O) linearization to explicitly account for the nonlinearities of the machine's current dynamics, yielding a linearized system representation that is controlled by PI-based state feedback. The controller parameters are tuned via linear quadratic regulation (LQR), enabling a systematic trade-off between stabilization and control effort. High-fidelity simulations demonstrate fast and accurate current tracking with significantly reduced cross-coupling compared to conventional state-feedback control.

Novelty: in contrast to state-of-the-art PI, state-feedback and predictive schemes, which all rely on linearized machine models, the proposed control framework

- is based on a generalized nonlinear SM model and explicitly accounts for nonlinear flux linkages,
- considers the back-EMF in the control law, and
- guarantees closed-loop stability through optimal (LQR) controller tuning.

System modeling & I/O linearization

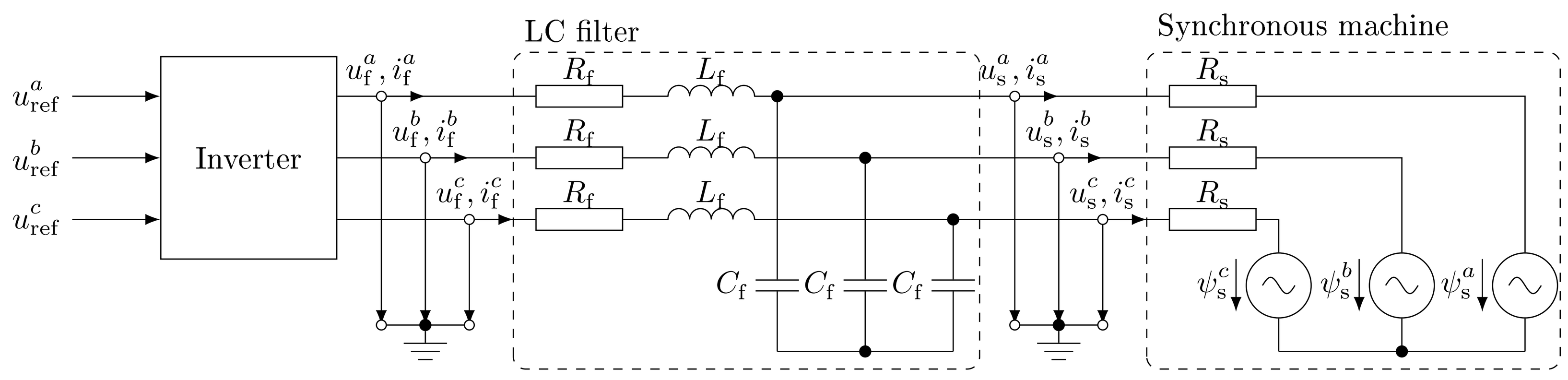

Fig. 1: Electrical drive system consisting of the inverter-side LC filter and the synchronous machine (voltages referenced to a common ground).

Filter dynamics [1] in the rotor-oriented (d, q)-reference frame, with filter voltages $\boldsymbol{u}_{\mathrm{f}}^{dq}$, currents $\boldsymbol{i}_{\mathrm{f}}^{dq}$, resistance R_{f}, inductance L_{f}, capacitance C_{f} and electrical angular velocity ω_{p}:

$$\left.\begin{aligned} \tfrac{\mathrm{d}}{\mathrm{d}t}\boldsymbol{i}_{\mathrm{f}}^{dq} &= -\tfrac{R_{\mathrm{f}}}{L_{\mathrm{f}}}\boldsymbol{i}_{\mathrm{f}}^{dq} - \omega_{\mathrm{p}}\boldsymbol{J}\boldsymbol{i}_{\mathrm{f}}^{dq} - \tfrac{1}{L_{\mathrm{f}}}\boldsymbol{u}_{\mathrm{s}}^{dq} + \tfrac{1}{L_{\mathrm{f}}}\boldsymbol{u}_{\mathrm{f}}^{dq}, \\ \tfrac{\mathrm{d}}{\mathrm{d}t}\boldsymbol{u}_{\mathrm{s}}^{dq} &= \tfrac{1}{C_{\mathrm{f}}}\boldsymbol{i}_{\mathrm{f}}^{dq} - \omega_{\mathrm{p}}\boldsymbol{J}\boldsymbol{u}_{\mathrm{s}}^{dq} - \tfrac{1}{C_{\mathrm{f}}}\boldsymbol{i}_{\mathrm{s}}^{dq}. \end{aligned}\right\}$$

Nonlinear machine model [2] with stator voltages $\boldsymbol{u}_{\mathrm{s}}^{dq}$, currents $\boldsymbol{i}_{\mathrm{s}}^{dq}$, resistance R_{s}, nonlinear flux linkages $\boldsymbol{\psi}_{\mathrm{s}}^{dq}(\boldsymbol{i}_{\mathrm{s}}^{dq})$ and differential inductance matrix $\boldsymbol{L}_{\mathrm{s}}^{dq} := \partial\boldsymbol{\psi}_{\mathrm{s}}^{dq}/\partial\boldsymbol{i}_{\mathrm{s}}^{dq}$:

$$\tfrac{\mathrm{d}}{\mathrm{d}t}\boldsymbol{i}_{\mathrm{s}}^{dq} = \boldsymbol{L}_{\mathrm{s}}^{dq}(\boldsymbol{i}_{\mathrm{s}}^{dq})^{-1}\big(\boldsymbol{u}_{\mathrm{s}}^{dq} - R_{\mathrm{s}}\boldsymbol{i}_{\mathrm{s}}^{dq} - \omega_{\mathrm{p}}\boldsymbol{J}\boldsymbol{\psi}_{\mathrm{s}}^{dq}(\boldsymbol{i}_{\mathrm{s}}^{dq})\big).$$

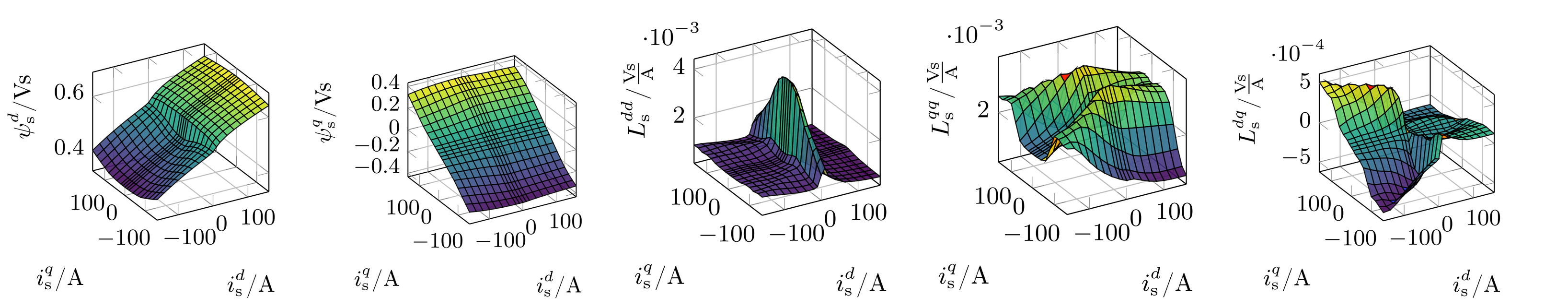

(a) (b) (c) (d) (e)

Fig. 2: FEA-based flux-linkage maps ψ_{s}^{d} (a), ψ_{s}^{q} (b) and differential inductance maps L_{s}^{dd} (c), L_{s}^{qq} (d), L_{s}^{dq} (e) in the (d, q)-current plane, illustrating magnetic saturation and cross-coupling.

Input/output linearization

With state $\boldsymbol{x} := ((\boldsymbol{i}_{\mathrm{f}}^{dq})^{\top}, (\boldsymbol{u}_{\mathrm{s}}^{dq})^{\top}, (\boldsymbol{i}_{\mathrm{s}}^{dq})^{\top})^{\top} \in \mathbb{R}^{6}$, input $\boldsymbol{u} := \boldsymbol{u}_{\mathrm{f}}^{dq}$ and output $\boldsymbol{y} := \boldsymbol{i}_{\mathrm{s}}^{dq}$, the system is control-affine, $\tfrac{\mathrm{d}}{\mathrm{d}t}\boldsymbol{x} = \boldsymbol{f}(\boldsymbol{x}) + \boldsymbol{g}(\boldsymbol{x})\boldsymbol{u}$. Differentiating $\boldsymbol{y}$ three times makes $\boldsymbol{u}$ appear explicitly and yields the linearizing control law

$$\boldsymbol{u} = \boldsymbol{K}_{\mathrm{lin}}(\boldsymbol{x})\boldsymbol{v} + \boldsymbol{u}_{\mathrm{lin}}(\boldsymbol{x})$$
$$\boldsymbol{K}_{\mathrm{lin}} := C_{\mathrm{f}}L_{\mathrm{f}}\boldsymbol{L}_{\mathrm{s}}^{dq}, \quad \boldsymbol{u}_{\mathrm{lin}} := L_{\mathrm{f}}(\boldsymbol{f}_3 - \boldsymbol{f}_1) + C_{\mathrm{f}}L_{\mathrm{f}}\big[\omega_{\mathrm{p}}\boldsymbol{J}(\boldsymbol{f}_2 + \dot{\boldsymbol{a}}) + R_{\mathrm{s}}\boldsymbol{\varphi}_3\big] - \boldsymbol{K}_{\mathrm{lin}}\big(\ddot{\boldsymbol{M}}\boldsymbol{a} + 2\dot{\boldsymbol{M}}\dot{\boldsymbol{a}}\big)$$

with $\boldsymbol{a} := \boldsymbol{u}_{\mathrm{s}}^{dq} - R_{\mathrm{s}}\boldsymbol{i}_{\mathrm{s}}^{dq} - \omega_{\mathrm{p}}\boldsymbol{J}\boldsymbol{\psi}_{\mathrm{s}}^{dq}$, $\boldsymbol{M} := (\boldsymbol{L}_{\mathrm{s}}^{dq})^{-1}$ and $\boldsymbol{\varphi}_3 := \boldsymbol{M}\dot{\boldsymbol{a}} + \dot{\boldsymbol{M}}\boldsymbol{a}$. Note that $\boldsymbol{u}_{\mathrm{lin}}$ contains the back-EMF; the derivatives of $\boldsymbol{M}$ are approximated by backward finite differences [3] with sampling time T_{s}. The closed loop then reduces to a chain of *triple integrators* in controllable canonical form, $\tfrac{\mathrm{d}}{\mathrm{d}t}\boldsymbol{z} = \boldsymbol{A}\boldsymbol{z} + \boldsymbol{B}\boldsymbol{v}$, $\boldsymbol{y} = \boldsymbol{C}\boldsymbol{z}$.

Control & validation

PI-based state feedback controller

The integrated control error $\boldsymbol{x}_i \in \mathbb{R}^2$, $\tfrac{\mathrm{d}}{\mathrm{d}t}\boldsymbol{x}_i = \boldsymbol{y}_{\mathrm{ref}} - \boldsymbol{C}\boldsymbol{z}$, extends the state to $\boldsymbol{\xi} = (\boldsymbol{z}^{\top}, \boldsymbol{x}_i^{\top})^{\top} \in \mathbb{R}^8$. The augmented system is controlled by

$$\boldsymbol{v} = -\boldsymbol{K}\boldsymbol{\xi} + \boldsymbol{L}\boldsymbol{y}_{\mathrm{ref}},$$

i.e. a classical PI controller combined with full-state feedback, optionally extended by anti-windup [4, Chap. 14]. The gain $\boldsymbol{K} := \boldsymbol{R}^{-1}\boldsymbol{B}_{\xi}^{\top}\boldsymbol{P}$ follows from the algebraic Riccati equation, so that all eigenvalues of $\boldsymbol{A}_{\xi} - \boldsymbol{B}_{\xi}\boldsymbol{K}$ lie in the open left complex half-plane. With normalized weightings, a single scalar $\alpha \in [0, 1]$ trades off state regulation against control effort, and $\boldsymbol{L} = \beta\boldsymbol{L}^{*}$, $\beta \in [0, 1]$, mitigates overshoot.

Validation

MATLAB/Simulink with a two-level VSI (ideal switching, space vector modulation, $u_{\mathrm{dc}} = 1.2\,$kV, $f_{\mathrm{sw}} = 10\,$kHz) and an FEA-based nonlinear SM ($81\,$kW, $3\,600\,$rpm). Reference current steps in the d- and q-axis are deliberately time-shifted to excite cross-coupling at rated speed. The PI-based state-feedback controller of [5] serves as baseline, tuned for comparable tracking dynamics.

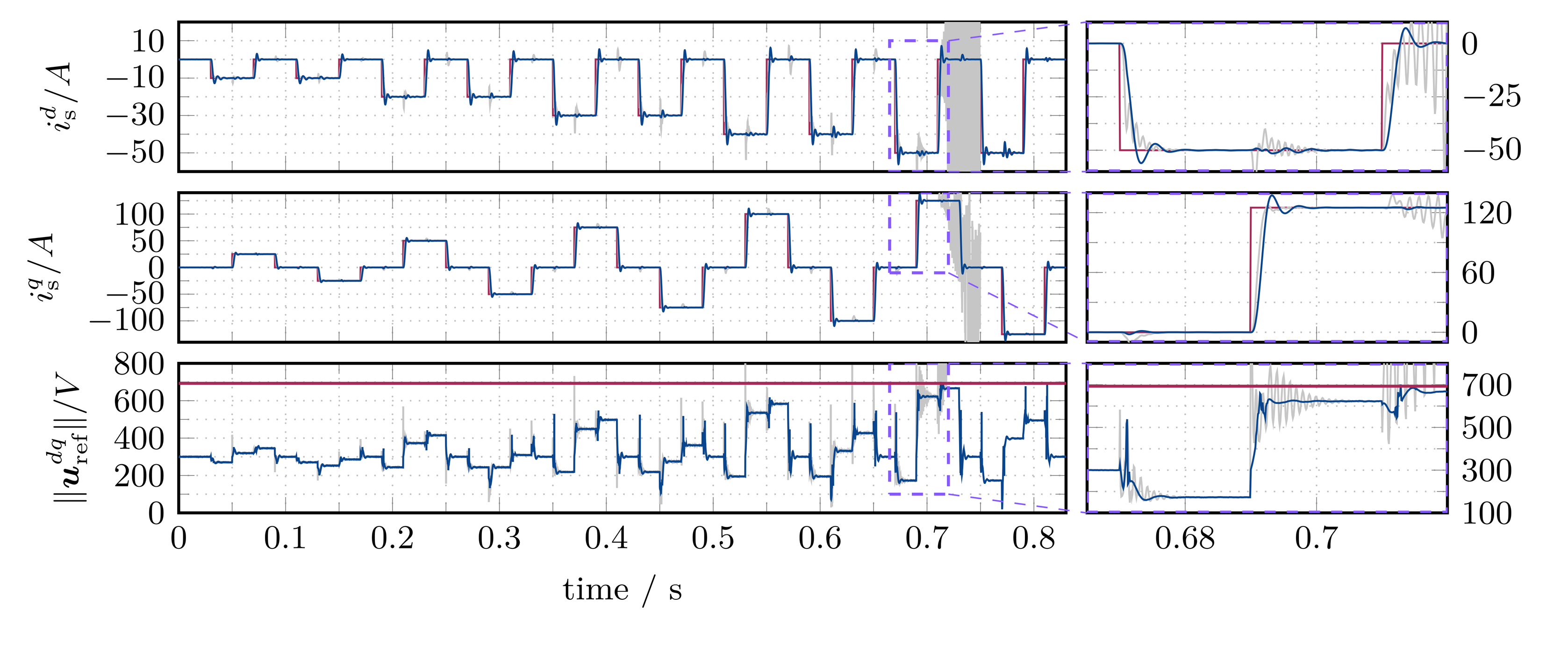

Fig. 3: Time-series results showing the (d, q)-currents and the reference voltage amplitude for the proposed controller [–] and a state-feedback controller [–], together with their reference values and the voltage limitation [–].

The proposed scheme achieves fast and accurate tracking with zero steady-state error, a settling time of approx. $5\,$ms and effectively compensated cross-coupling. The state-feedback baseline exhibits pronounced cross-coupling in i_{s}^{d} and becomes unstable at $t = 0.71\,$s, demonstrating that the linearized model assumption may fail under strongly nonlinear operating conditions.

Conclusion & References

Exact I/O linearization turns the cascaded filter–machine system into a chain of triple integrators, regulated by PI-based state feedback with LQR tuning. It tracks fast and accurately, strongly reduces cross-coupling and stays stable where linear state feedback fails. Future work: state observer, robustness analysis, experimental validation.

[1] J. Kullick and C. Hackl, "Dynamic Modeling and Simulation of Deep Geothermal Electric Submersible Pumping Systems," *Energies*, vol. 10, p. 1659, Oct. 2017.
[2] N. Monzen and C. M. Hackl, "Optimal reference voltage saturation for nonlinear current control of synchronous machine drives," *IEEE Transactions on Industry Applications*, vol. 62, pp. 1029–1038, Jan. 2026.
[3] J. Li, "General explicit difference formulas for numerical differentiation," *Journal of Computational and Applied Mathematics*, vol. 183, pp. 29–52, Nov. 2005.
[4] C. M. Hackl, *Non-identifier based adaptive control in mechatronics: Theory and Application*. No. 466 in Lecture Notes in Control and Information Sciences, Berlin: Springer International Publishing, 2017.
[5] J. Kullick and C. M. Hackl, "Speed-sensorless control of induction machines with LC filter for geothermal electric submersible pumping systems," *Machines*, vol. 10, no. 2, p. 87.